Raman Modes of MoS_2 Used as Fingerprint of van der Waals Interactions in 2-D Crystal-Based Heterostructures

Kai-Ge Zhou,[†] Freddie Withers,[‡] Yang Cao,[‡] Sheng Hu,[‡] Geliang Yu,[‡] and Cinzia Casiraghi*[,†]

[†]School of Chemistry and [‡]School of Physics and Astronomy, University of Manchester, Oxford Road, Manchester M13 9PL, U.K.

ABSTRACT In this work, we use Raman spectroscopy as a nondestructive and rapid technique for probing the van der Waals (vdW) forces acting between two atomically thin crystals, where one is a transition metal dichalcogenide (TMDC). In this work, MoS_2 is used as a Raman probe: we show that its two Raman-active phonon modes can provide information on the interaction between the two crystals. In particular, the in-plane vibration (E_{2g}^1) provides information on the in-plane strain, while the out-of-plane mode (A_{1g}) gives evidence for the quality of the interfacial contact. We show that a vdW contact with MoS_2 is characterized by a blue shift of $+2$ cm^{-1} of the A_{1g} peak. In the case of a MoS_2/graphene heterostructure, the vdW contact is also characterized by a shift of $+14$ cm^{-1} of the 2D peak of graphene. Our approach offers a very simple, nondestructive, and fast method to characterize the quality of the interface of heterostructures containing atomically thick TMDC crystals.

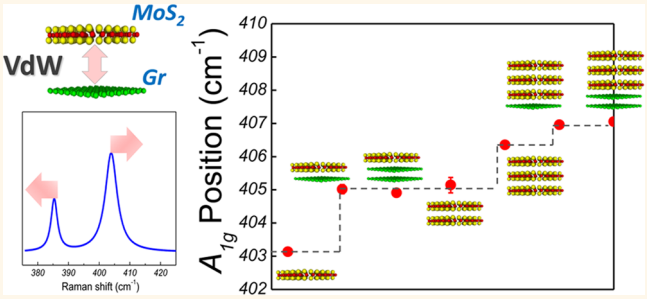

KEYWORDS: heterostructures · 2D crystals · van der Waals interaction · strain · Raman spectroscopy · MoS_2

Heterojunctions have played a critical role in electronic devices, such as transistors, rectifiers, quantum wells, photoelectric converters, *etc.*[1] Most heterostructures consist of two materials in close contact either through ionic bonding or by van der Waals (vdW) interaction. It is well-known that strong effects can occur at the interface between these materials, which may result in a dramatic variation of the device performance.[2]

The very recent discovery of a new class of materials, two-dimensional (2-D) crystals such as graphene, MoS_2, WS_2, and boron nitride (BN), *etc.*,[3] has led to the development of 2-D crystal-based heterostructures,[4−13] composed of individual atomic crystals stacked on top of each other. Therefore, the whole heterostructure is held together by vdW interactions. Such novel heterostructures show great promise for flexible and transparent electronic and optoelectronic applications. However, the fabrication process is quite complex and requires several mechanical transfer processes, where polymers and solvents are used in order to transfer a crystal on top of another.[14] Because of this, the heterostructures can often suffer from contamination trapped at the interface, typically coagulating in the form of bubbles.[14−16] Interfacial strain and contamination can strongly affect the performance of the device.[14] Therefore, it is very important to be able to characterize the contact between the crystals.

Normal surface techniques, for instance, scanning probe microscopy or contact angle measurements, are only sensitive to the top layer, but they are unable to probe the properties of the interface. Currently, the only method able to provide information on the morphology of the interface is cross-sectional high-resolution transmission electron microscopy.[14] However, this method is time-consuming and destructive. Therefore, it is essential to develop a fast, simple, and nondestructive technique that can be easily implemented into the device fabrication processes.

Raman spectroscopy is a powerful tool for the noninvasive characterization of graphene and other 2-D crystals.[17−25] This technique has been also used to identify and quantify the quality of the interface in epitaxial multilayers, where effects of strain

* Address correspondence to cinzia.casiraghi@manchester.ac.uk.

Received for review February 18, 2014 and accepted September 8, 2014.

Published online September 08, 2014
10.1021/nn5042703

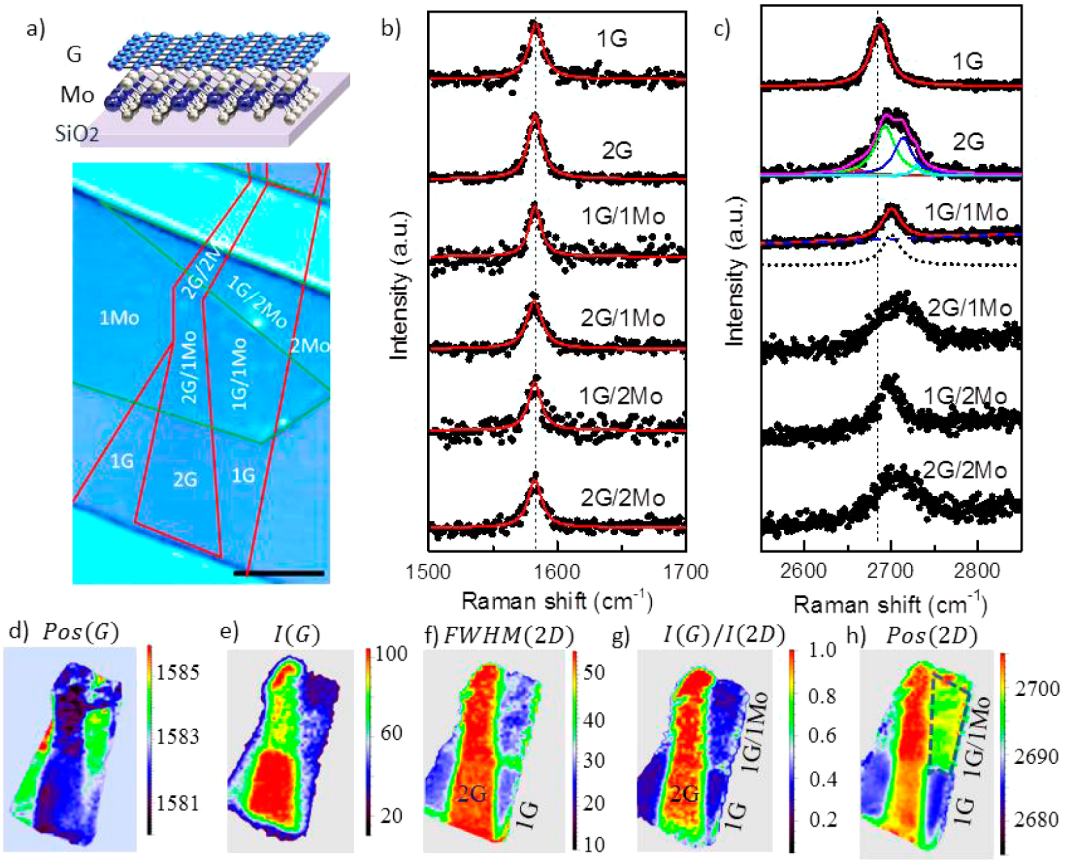

Figure 1. (a) Optical image of *n*G/*m*Mo heterostructures on Si/SiO_2 (*n* = 1, 2; *m* = 1, 2). The scale bar is 5 μm. The region marked by the green line corresponds to single-layer MoS_2, while the zone surrounded by the red line represents the graphene and bilayer area. (b) G and (c) 2D bands of graphene measured for different heterostructures. The dots correspond to the experimental data, while the solid lines indicate the fits obtained by using a Lorentzian line shape. (d–h) Raman maps of the G peak position, its intensity, its full width at half-maximum, intensity ratio between G and 2D peaks, and 2D peak position, respectively.

and dislocations must be minimized to create perfect heterostructures from materials with different lattice parameters.[24,26] In this work, we combine these two approaches to overcome the challenge of characterizing the interface between a transition metal dichalcogenide (TMDC) and another 2-D crystal. Our strategy is to apply a "knock-listen" method. In this scheme, the vibration of one component of the heterostructure interface is first stimulated (*i.e.*, "knock") by an external wave (*i.e.*, a light beam), and the effect can be directly measured by collecting the inelastically scattered light (*i.e.*, "listen"). To test our strategy, we investigated several heterostructures where molybdenum disulfide (MoS_2) monolayer is used as a probe to extract information about the contact at the interface. The Raman spectrum of MoS_2 shows two main Raman-active modes, $E_{2g}{}^1$ and A_{1g}.[27−30] The $E_{2g}{}^1$ mode represents an in-plane vibration, and the A_{1g} mode corresponds to an out-of-plane lattice expansion. According to the thickness-dependence Raman studies,[28,29] the out-of-plane Raman vibration depends on the interaction with its neighboring material; hence this Raman mode should provide information on the strength of the vdW interaction between the two adjacent layers.

In this work, we present a variety of heterostructures containing MoS_2 crystals. To clearly describe all the heterostructures investigated, we refer to them in the following way: "*n*X/*m*Y" describes a heterostructure in which *n* and *m* represent the number of layers, and X and Y describe the top and bottom crystals, respectively. The number of layers has been identified by using a combination of optical and Raman spectroscopy.[28−30] In all cases, the heterostructure lies on silicon covered by a 290 nm oxide layer substrate (Si/SiO_2). Note that the samples are made in such a way that the layers X and Y also partially lie on the bare substrate, so their corresponding Raman spectra can be used as a reference to reveal the effects of the interfacial contacts. In order to avoid effects from uncontrolled and unwanted doping, strain, and defects, we used high-quality flakes produced by micromechanical exfoliation, and we optimized the transfer process to minimize residuals trapped at the interface.[14]

RESULTS AND DISCUSSION

Figure 1a shows an optical micrograph of *n*G/*m*Mo heterostructures on Si/SiO_2 (*n* = 1, 2; *m* = 1, 2), where G refers to graphene and Mo to MoS_2. We first focus on

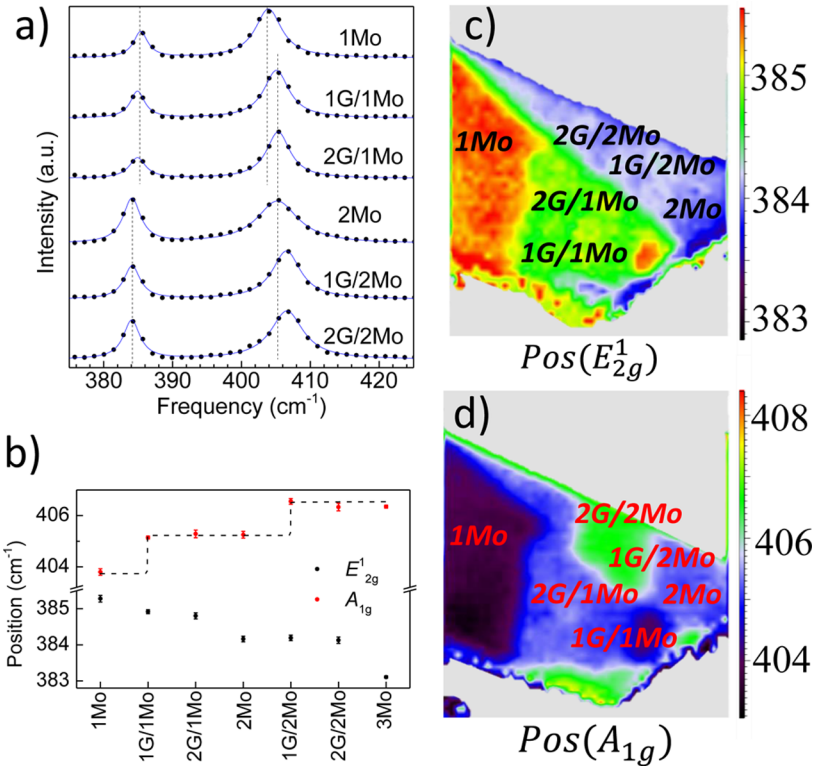

Figure 2. (a) Raman spectrum of MoS_2 in a *n*G/*m*Mo heterostructure on Si/SiO_2 (n = 1, 2; m = 1, 2), as shown in Figure 1a. The dots correspond to the experimental data, while the solid lines are the fits obtained by using a Lorentzian line shape. (b) Raman peaks positions of MoS_2 extracted from the spectra in (a). Raman maps of (c) E_{2g}^1 and (d) A_{1g} positions for the heterostructures depicted in Figure 1. Note that the red and green regions in (c) correspond to bare MoS_2 and encapsulated MoS_2, respectively. In (d), the dark blue region (403.8 cm^{-1}) corresponds to bare monolayer MoS_2 (1Mo), while encapsulated MoS_2 (1G/1Mo and 2G/1Mo) corresponds to the light blue region (405.2 cm^{-1}), which also extends to bilayer MoS_2 (2Mo).

the Raman spectrum of graphene. Figure 1b compares the G band of graphene and its bilayer on bare Si/SiO_2 and the G band measured in the heterostructures. The G peak position is 1583−1584 cm^{-1} in all cases, showing no remarkable difference between graphene on MoS_2 and Si/SiO_2, in agreement with the Raman map of the G band in Figure 1d. The full width at half-maximum (fwhm) of the G peak also shows negligible change if graphene is deposited on Si/SiO_2 or on MoS_2 (Figure S2, Supporting Information). Figure 1c shows the second-order Raman spectrum of graphene: the 2D band shows a blue shift from 2685 cm^{-1} for bare graphene to 2699 cm^{-1} when transferred on MoS_2. This is evident from the Raman map of the 2D peak shown in Figure 1h (the yellow-green region surrounded by the dashed line). The shift appears to be independent of the number of MoS_2 layers beneath graphene. Independent of the substrate, the 2D fwhm is 27 cm^{-1} for monolayer graphene (Figure 1f). Concerning the intensity, the G and 2D peak intensities are strongly reduced when graphene is placed on MoS_2, which is clearly seen in the Raman map shown in Figure 1d. The decrease of the band intensity is attributed to interference effects and absorption of MoS_2.[31−34] However, the intensity ratio between the G and 2D peaks is not affected by the substrate, as shown in Figure 1g. Therefore, the width of the 2D band and I_G/I_{2D} are still suitable parameters for identification of monolayer graphene in heterostructures.

We now focus on the Raman spectrum of MoS_2. Figure 2a compares the spectrum of single-layer and bilayer MoS_2 in contact only with the Si/SiO_2 substrate, with the spectrum of MoS_2 encapsulated between graphene and the substrate (Figure 1a). Figure 2b shows that both the Raman peaks of MoS_2 shift when the layer is encapsulated. The additional layer of graphene causes the E_{2g}^1 peak to slightly shift from 385 to 384 cm^{-1} (green region in Figure 2c) and the A_{1g} to shift from 403 to 405 cm^{-1} (white region in Figure 2d). Those positions do not change when a second layer of graphene is transferred on top. This indicates that the shifts of E_{2g}^1 and A_{1g} are caused only by the direct contact with graphene and not by the number of graphene layers placed on top of MoS_2. Similarly, for bilayer MoS_2, its encapsulation in one or two layers of graphene causes a blue shift of A_{1g} from 405 to 406.5 cm^{-1} (white region in Figure 2d); also, in this case, the effect does not depend on the number of graphene layers used as a top layer. Similar blue shifts have been found in other graphene/MoS_2 heterostructures (Figure S3, Supporting Information).

In order to understand these results, one has to note that the changes in the E_{2g}^1 and A_{1g} positions observed in encapsulated MoS_2 are similar to the shift in the

positions observed when increasing the thickness from single-layer MoS_2 to few-layer MoS_2.[28,29] In particular, the A_{1g} position of *n*G/1Mo (n = 1, 2) at 405.1 cm^{-1} matches that of a bare bilayer MoS_2 (405.2 cm^{-1}) (Figure 2b). The Raman map of the A_{1g} position does not show any difference between *n*G/1Mo (n = 1, 2) and 2Mo (Figure 2d). A similar result is found for *n*G/2Mo (n = 1, 2) and trilayer MoS_2 (A_{1g} position is 406.4 cm^{-1}). According to above facts, we can conclude that

$$\mathrm{Pos}_{mG/n\mathrm{Mo}}(A_{1g}) \approx \mathrm{Pos}_{(n+1)\mathrm{Mo}}(A_{1g}) \quad (m = 1, 2, \ldots; n = 1, 2, 3, \ldots) \quad (1)$$

where $\mathrm{Pos}(A_{1g})$ is the position of the A_{1g} peak in a *m*G/*n*Mo heterostructure and in a thin layer MoS_2 [(*n*+1)Mo]. We attribute this result to the different nature of the vibrations involved when MoS_2 is encapsulated into a heterostructure. The position of a phonon with momentum $\mathbf{q}$, Pos($\mathbf{q}$), in a condensed material can be written as[30]

$$\left| \frac{1}{\sqrt{M_I M_J}} \sum C_{I\alpha, J\beta}(\mathbf{q}) - \mathrm{Pos}^2(\mathbf{q}) \right| = 0 \quad (2)$$

where M_I and M_J are the masses of the atoms I and J involved in the vibration, and $C_{I\alpha,J\beta}(\mathbf{q})$ corresponds to the real-space atomic force constant matrix, where α and β represent the direction of the atoms I and J displacement, respectively. For the $E_{2g}{}^1$ mode of MoS_2, the dominant in-plane long-range interaction term, $C_{\mathrm{Mo}_x\mathrm{Mo}_x}$ will decrease with increasing number of layers or lattice expansion.[30] Therefore, the decrease in $C_{\mathrm{Mo}_x\mathrm{Mo}_x}$ causes softening of the $E_{2g}{}^1$ mode. Meanwhile, owing to the additional interlayer interaction term, the matrix elements $C_{Sz,Sz'}$ will increase and cause a blue shift of the A_{1g} mode as observed with increasing number of MoS_2 layers.[30]

By using this model, given that the $E_{2g}{}^1$ mode has a small shift of -1.3 cm^{-1} as compared to the bare MoS_2, and that the Gruneisen parameter of the $E_{2g}{}^1$ mode is 0.54,[35] we found that a 0.3% lattice expansion occurs for MoS_2. However, while the position of the $E_{2g}{}^1$ mode keeps changing with increasing MoS_2 thickness, its position does not change with increasing number of graphene layers in the heterostructure, indicating that the in-plane stretching only comes from the interfacial contact with graphene. In addition, the interlayer strain can also be identified in graphene: when graphene is placed on MoS_2, the 2D peak shifts $+14$ cm^{-1} as compared to the bare graphene (Figure 1c). This corresponds to a 0.1% in-plane compression by using a 2D peak Gruneisen parameter of 2.6 (see also Supporting Information).[36] This is in agreement with recent *ab initio* simulations, in which the C−C bonds are expected to shrink from 1.41 to 1.40 Å in a graphene−MoS_2 superlattice.[37] According to the shift of $E_{2g}{}^1$ and 2D modes measured when graphene and MoS_2 are in direct contact, MoS_2 appears to be stretched, while graphene is slightly compressed. Therefore, we can use the shift of $E_{2g}{}^1$ and the 2D modes to get direct information on the interfacial strain of the crystals in contact in the heterostructure. We observed the same 2D peak shift in high mobility BN/1G/Mo heterostructures, where graphene is encapsulated between thick layers of hexagonal boron nitride (BN) and MoS_2 (Supporting Information). In contrast, low-mobility BN/1G/MoS_2 heterostructures show a 2D peak shift of $+5$ cm^{-1}, showing that the lower quality of the contact between the crystals can significantly affect the performance of the device (Supporting Information, Figure S8).

Concerning the out-of-plane A_{1g} mode, the shift observed in the heterostructures can be attributed to the interlayer interaction between graphene and MoS_2. For bare MoS_2, the interaction term $C_{Sz,Sz}$ within one layer dominates the out-of-plane A_{1g} mode. This term can be modeled as a "spring" connecting the two sulfur layers (Figure 3). Without spatial restriction from the environment, the spring has full freedom to oscillate, so for a bare MoS_2 monolayer, the phonon position of A_{1g} is equal to $[(1/M_s)(C_{Sz,Sz})]^{1/2}$ (eq 2). However, the loading of a graphene layer introduces a vdW term, $C_{Sz,Cz'}$, into the total interaction matrix. Owing to this additional spring, the phonon position of A_{1g} will increase up to $[(1/M_s)(C_{Sz,Sz} + C_{Sz,Sz'})]^{1/2}$. This additional term is negligible above 4 Å,[38] so the term $C_{Sz,Cz'}$ is a fingerprint of the vdW interaction of the neighboring 2-D crystals. This explains why the shift of the A_{1g} mode is independent of the numbers of graphene layers in the heterostructure. This can be used as a fingerprint of the vdW interaction strength in our heterostructure: from eq 1, we know that the A_{1g} phonon position of G/1Mo nearly equals that of 2Mo, indicating that $(C_{Sz,Sz} + C_{Sz,Cz'}) \approx (C_{Sz,Sz} + C_{Sz,Sz'})$. Therefore, the interlayer vdW interaction at the interface with graphene ($C_{Sz,Cz'}$) is as strong as that between MoS_2 ($C_{Sz,Sz'}$). This result shows that if no shift or a small shift of the A_{1g} peak is observed after contact, then the stacking interaction is not of high quality, and further techniques shall be developed to improve the interfacial contact. Therefore, this method can be very useful in the prescreening of the quality of the heterostructures. However, one could argue that in our case the shift may be produced by other effects. Owing to the change on the anharmonic terms in the lattice potential energy of MoS_2, the laser-induced thermal effect can be very strong.[39,40] However, the thermal effect would be the same for graphene and MoS_2 on the substrate and in the heterostructure, in particular, considering the very small attenuation of the laser power through 1 or 2 graphene layers. Furthermore, both MoS_2 modes should harden for increasing temperature.[39,40] However, in our study, the $E_{2g}{}^1$ mode was found to soften. This allows us to exclude any thermal effect. Note that damage by heating was observed only in

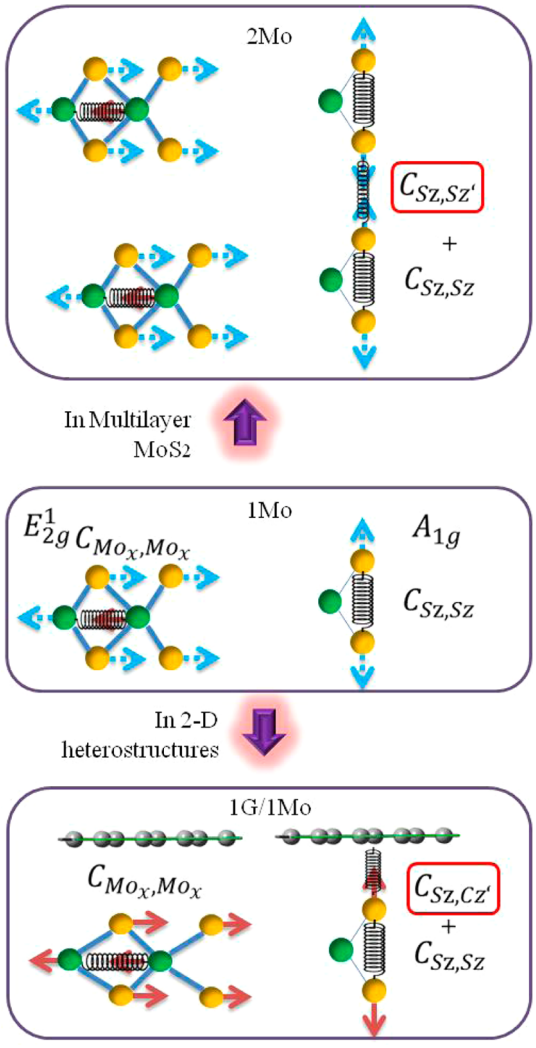

Figure 3. Schematic of the interaction between graphene and MoS_2 in a heterostructure 1G/1Mo (bottom panel), as compared to 1Mo (middle panel) and 2Mo (top panel). The green, gold, and gray balls represent molybdenum, sulfur, and carbon atoms, respectively. The arrows indicate the direction of atom displacement (*x* or *z*). The dominating interaction terms $C_{l\alpha,J\beta}$ for the $E_{2g}{}^1$ and A_{1g} mode are modeled by using springs.

suspended heterostructures (Figure S5, Supporting Information).

Another effect that can shift the Raman peaks is doping: this has been observed in both graphene[41] and MoS_2.[42] One should consider doping from the charged impurities in the Si/SiO_2 substrate[43,44] and from charge transfer between graphene and MoS_2. Note that the Raman peaks of graphene are strongly sensitive to doping, in particular, the G peak, because of the removal of the Kohn anomaly at the Γ point.[45] However, the effect of doping is expected to be smaller in other materials such as MoS_2. Indeed, a shift of 4 cm^{-1} is observed for the A_{1g} mode for a charge concentration of 1.8×10^{13} cm^{-2},[42] in contrast to a shift of 10 cm^{-1} for the G peak at the same charge concentration.[41] The G peak position in our heterostructure is found to be at ~1583 cm^{-1}, corresponding to a very small charge concentration (well below 10^{13} cm^{-2}), suggesting that graphene is slightly doped (Fermi energy ≪ 0.2 eV), which is a typical condition for graphene exposed to atmospheric conditions. Recent studies also showed that the Raman signals on the suspended MoS_2 have no significant difference from those on Si/SiO_2,[29,46] showing that the effect of MoS_2 doping from the substrate is negligible. Concerning charge transfer, it has been shown that in order to achieve doping levels high enough to be probed by Raman spectroscopy, MoS_2 must contains heavy metal impurities.[47] Therefore, it is reasonable not to expect any effect from charge transfer in the Raman spectrum of MoS_2 on graphene. In addition, doping would affect also the intensity ratio between 2D and G peaks, I_G/I_{2D},[41,48−50] in contrast to our results, where no strong variations in this parameter have been observed (Figure 1g). Therefore, doping should have a negligible effect on the shift of the peaks observed in our heterostructures.

Because we can neglect external perturbations such as doping and heating, the shift of 2 cm^{-1} of the A_{1g} mode is taken as a fingerprint of the vdW contact. In the general case, where one cannot neglect effects from external perturbations, it can be useful to analyze the Raman peaks from both crystals in the heterostructure. For example, in the case of a Gr/MoS_2 heterostructure, a vdW contact will be characterized by a blue shift of ~2 cm^{-1} for the A_{1g} peak and a blue shift of ~14 cm^{-1} for the 2D peak (Figure 1c).

The loading-induced blue shift of the A_{1g} mode for MoS_2 bilayer can be understood in the same way: when bilayer MoS_2 is encapsulated by graphene, the total interaction term further increases, so the position of the A_{1g} mode further blue shifts, closer to that in trilayer MoS_2. Therefore, the blue shift of the A_{1g} mode of single-layer or bilayer MoS_2 encapsulated by graphene is also attributed to the vdW interaction. However, we do not see any effect when graphene is placed on tri- or multilayer MoS_2. This can be explained by taking into account that the interface is now giving a smaller contribution to the overall Raman signal.

Since MoS_2 is found to be stacked naturally, the packing between graphene and MoS_2 is certainly self-stimulated from thermodynamics. This self-driven stacking makes the formation of 2-D heterostructures possible,[4,11,16] and the observed vdW terms here can also explain the driving force in the chemical vapor growth of MoS_2 on graphene.[12]

The second type of heterostructure is *n*Mo/*m*G (*n* = 1, 3; *m* = 1, 2) (Figure 4a). In this case, graphene is encapsulated between the substrate and MoS_2. Figure 4b,c shows the first and second order of the graphene Raman spectrum, respectively. Similar to *n*G/*m*Mo, the position of the 2D band has a blue

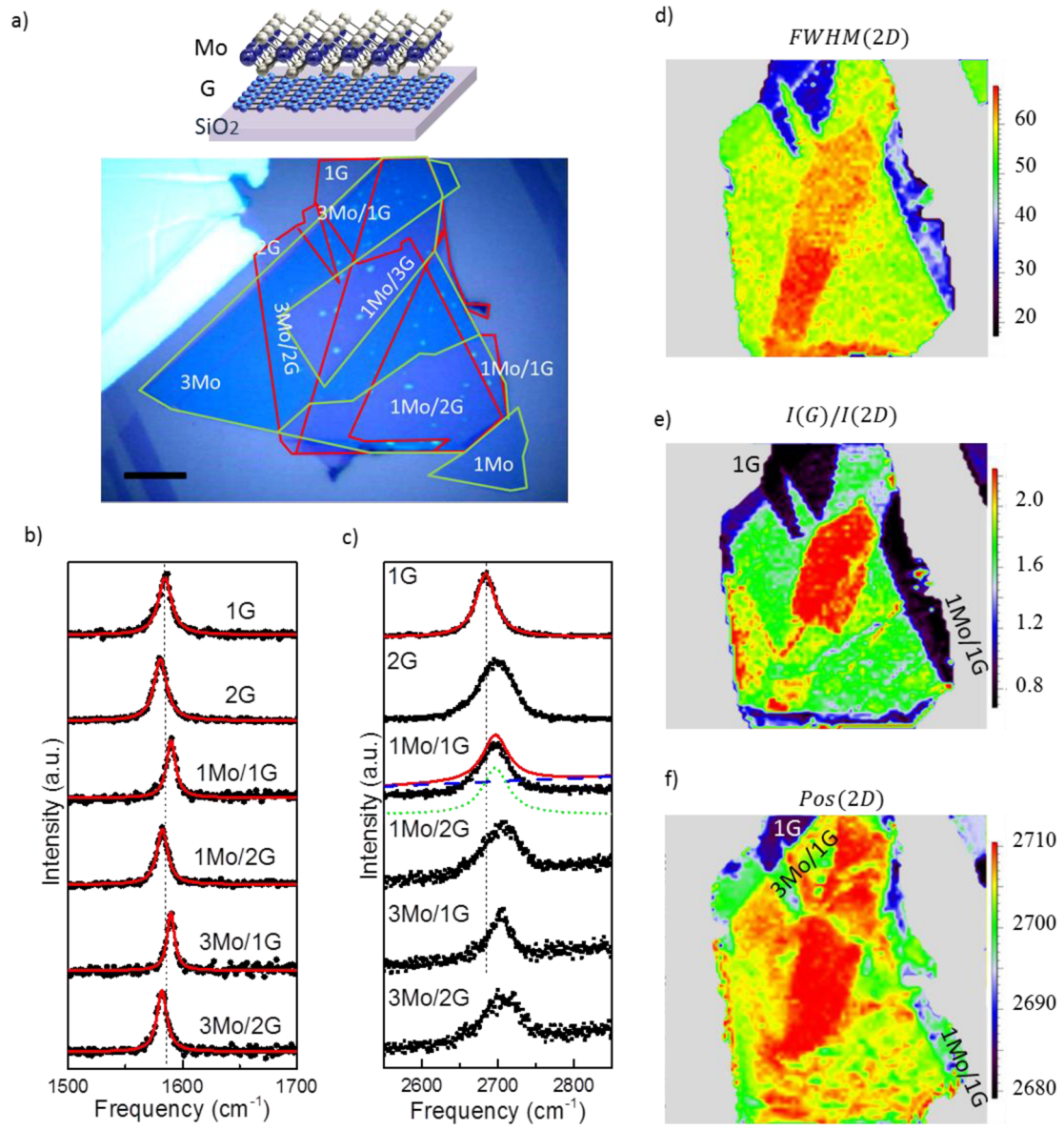

Figure 4. (a) Optical image of *n*Mo/*m*G (*n* = 1, 3; *m* = 1, 2) heterostructures (the scale bar is 10 μm). The region marked by the green line corresponds to *n* layers MoS_2, while the zone surrounded by the red line represents *m* graphene layers. (b) G and (c) 2D bands of graphene measured for different heterostructures. The dots correspond to the experimental data, while the lines indicate the fitting obtained by using a Lorentzian line shape. (d–f) Raman maps of fwhm (2D), I_{2D}/I_G, and the position of the 2D band, respectively.

shift of +13 cm^{-1} from 2683 (bare) to 2696 cm^{-1} under MoS_2, indicating a 0.9% in-plane compression of graphene.[36] One might note that in *n*Mo/1G (*n* = 1, 3), the G band has a blue shift of 5 cm^{-1} (from 1585 to 1590 cm^{-1}), compared to the bare graphene, while in the *n*G/*m*Mo heterostructure, we did not observe any strong shift. This difference can be due to the higher sensitivity of graphene to the neighboring materials, for example, due to different dielectric environments on the top and bottom layers. A shift in the G peak has been observed in all heterostructures where graphene is encapsulated between two crystals (Figure S7) and its origin is not completely understood.

In a MoS_2 monolayer (1Mo), the position of the $E_{2g}{}^1$ and A_{1g} modes are at 384.9 and 403.1 cm^{-1}, respectively (Figure 5a). When monolayer MoS_2 is placed on mono- or bilayer graphene, the $E_{2g}{}^1$ mode is softened by about 1 cm^{-1}. The A_{1g} phonon of monolayer MoS_2 has a blue shift of about 2 cm^{-1} on Mo/*m*G heterostructures (*m* = 1, 2) (Figure 5). Likewise, the $E_{2g}{}^1$ and A_{1g} modes of bi- and trilayer MoS_2 were also found to shift to opposite directions on graphene. The distance between $E_{2g}{}^1$ and A_{1g} modes was found to vary from 18.2 (white blue region in Figure S1b) to 20.7 cm^{-1} (green region in Figure S1b). Since eq 2 is still valid for mono- to trilayer MoS_2 on graphene, this shift indicates the existence of a vdW interaction at the interface.

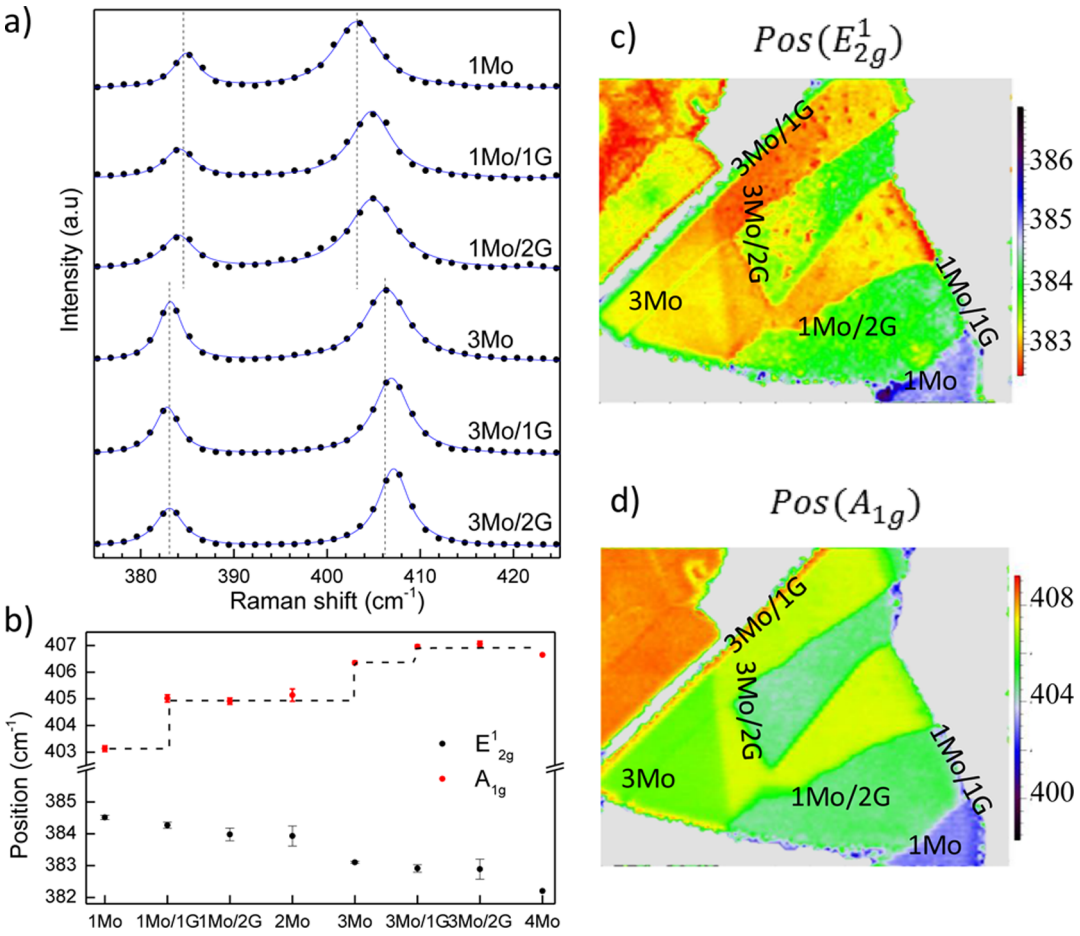

Figure 5. (a) Raman spectra of MoS_2 in *n*Mo/*m*G heterostructures. The dots correspond to the experimental data, while the solid lines are the fits obtained by using a Lorentzian line shape. (b) MoS_2 peak positions extracted from the spectra in (a). The peak positions for bi- and four-layer MoS_2 in (b) are extracted from Figure 2a and ref 29. The Raman maps of the position of the (c) E_{2g}^1 and (d) A_{1g} modes for the heterostructures in Figure 4.

Similar blue shifts of A_{1g} and 2D bands are reproducible in other MoS_2/graphene heterostructures (Figure S3, Supporting Information). Similar to the results demonstrated for the *n*G/*m*Mo heterostructures, the shifts are not affected by the number of graphene layers used as bottom layers. Thus, our model is valid in both heterostructures when MoS_2 is encapsulated or used as a top layer.

In order to extend our model to other types of heterostructures, we replaced graphene with mica. This is an interesting substrate because it is able to enhance the luminescence of a MoS_2 monolayer,[51] and therefore, it shows great potential in light-emitting devices. Here we apply our approach to probe the contact in MoS_2/mica heterostructures. In this case, in contrast to the heterostructures previously investigated, we can only use the Raman-active phonon of MoS_2 to analyze the interfacial contact since the Raman signal of mica is too weak to be observed under our experimental conditions.

Figure 6b shows that the E_{2g}^1 peak of MoS_2 on the mica substrate has a meaningless shift of 0.2 cm^{-1} (below the resolution of the spectrometer) compared to the bare MoS_2. However, for the A_{1g} mode, the monolayer MoS_2 on mica initially shows a blue shift of 1.1 cm^{-1} as compared to the bare sample, suggesting a vdW interaction. However, the position of this mode is not uniform, indicating that the contact is not perfect. It is also noted that the blue shift of A_{1g} on mica (0.9 cm^{-1}) is smaller than that shift observed in graphene heterostructures. Therefore, the initial vdW term, $C_{Sz,micaz'}$ is weaker than $C_{Sz,Cz'}$, indicating that the interfacial contact is not as good as in the graphene heterostructures previously investigated. In such a case, the contact can be regarded as a "pseudo-soldering". In order to improve the contact, we used atomic force microscopy (AFM). After AFM tapping, the E_{2g}^1 peak remains at the same position, while the A_{1g} mode upshifts and becomes closer to that of bilayer MoS_2 (Figure 6c). Moreover, the pseudo-soldering disappears, indicating that the MoS_2/mica contact can be improved by AFM and probed by Raman spectroscopy. Note that the total A_{1g} shift, however, is still below 2 cm^{-1}, indicating that mica is not a good substrate for fabrication of heterostructures composed of micromechanically exfoliated 2-D crystals, in agreement with

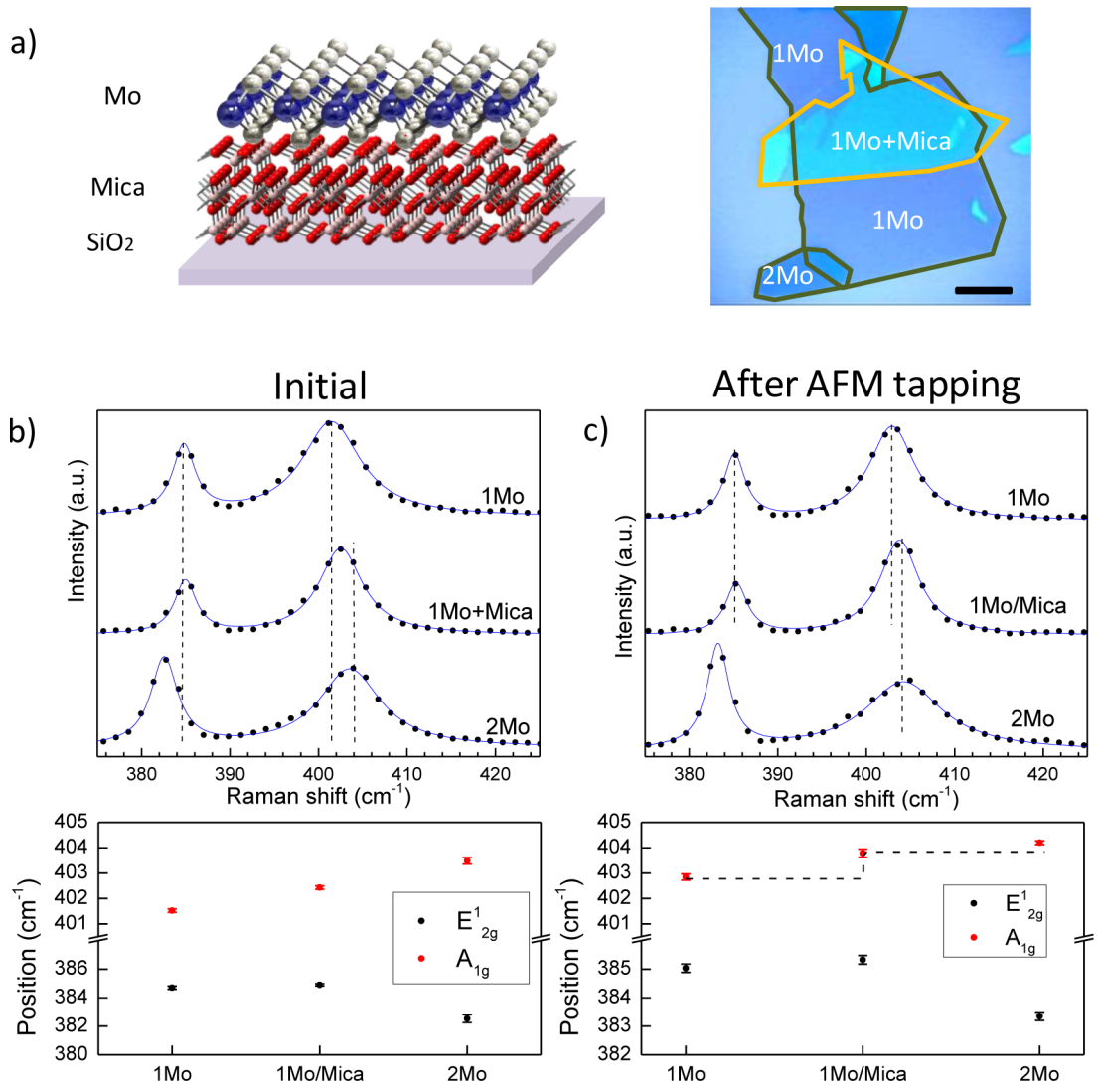

Figure 6. (a) Schematic and optical image of 1Mo/mica heterostructure (the scale bar is 10 μm). The region marked by the green line corresponds to MoS_2, while the zone surrounded by the orange line represents the mica. (b) Raman spectra of 1Mo/mica heterostructures shown in (a). (c) Raman spectra of Mo/mica heterostructures after tapping the surface. The dots correspond to the experimental data, while the solid lines are the fits obtained by using a Lorentzian line shape.

recent results.[14] Our method for probing the interfacial contact can be applied to all two-dimensional materials with significant in- and out-of-plane vibration modes, such as WS_2, WSe_2, $MoSe_2$, $NbSe_2$, VS_2, Bi_2Te_3, $TaSe_2$, and GaSe. In the Supporting Information, we show additional results on a graphene/WS_2 heterostructure (Figure S4); also, in this case, we observed the A_{1g} peak of the WS_2 blue shift when WS_2 is encapsulated in the heterostructure.

We finally show that our method can be used to also characterize heterostructures made of different TMDCs, making our method completely general (the heterostructure, however, must contain at least an atomically thin TMDC). Figure 7a shows a heterostructure composed by a single-layer MoS_2 and WS_2: 1Mo/1W. This type of heterostructure has attracted an increasing level of attention due their potential use in photovoltaic devices and rectifiers.[52−55]

We first analyze the vdW effect on the A_{1g} mode of MoS_2. As shown in Figure 7b, the position of the A_{1g} peak is higher in the 1Mo/1W heterostructure (the green region) than in 1Mo (the dark blue region). Compared to the MoS_2 monolayer, its A_{1g} peak is hardened by $+2$ cm^{-1} in 1Mo/1W (Figure 7c). This is in agreement with the results obtained for 1Mo/G and G/1Mo heterostructures (Figures 2 and 4). In addition, the A_{1g} mode of WS_2 shows a blue shift of $+1$ cm^{-1}, which is in agreement with the results observed in the 1W/1G heterostructure (Figure S4, Supporting Information).

One may argue that the blue shift of the A_{1g} mode in the 1Mo/1W heterostructure could come from the photogenerated charge transfer between MoS_2 and WS_2. This would correspond to a p-doping of 0.9×10^{13} cm^{-2} in MoS_2.[42] However, as recently demonstrated by Wang *et al.*,[52] a hole concentration of 0.5×10^{13} cm^{-2} can be

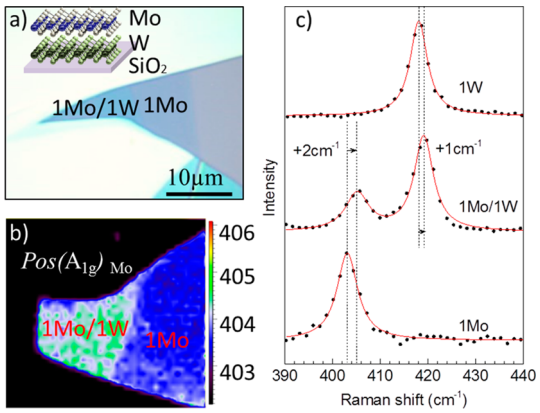

Figure 7. (a) Schematic and optical image of 1Mo/1W heterostructure placed on Si/SiO_2 (the scale bar is 10 μm). (b) Raman mapping of Mo/W heterostructures. (c) Typical Raman spectra of 1Mo/1W heterostructures extracted from (b). The dots correspond to the experimental data, while the solid lines are the fits obtained by using a Lorentzian line shape. Note that the spectrum of 1W is collected under the same conditions of the sample in Figure S4a of the Supporting Information.

pumped from MoS_2 to WS_2 by an incident pulse laser about 1W. Considering the low power (50 μW) in our experiment, the photogenerated charge transfer is not strong enough to be observed by Raman. Therefore, the photogenerated charge transfer is not compatible with the shift of the A_{1g} mode.

In principle, several other phonons can also be used as an alternative contact probe. For instance, the shearing and breathing modes can be treated as in- and out-of-plane vibration modes, respectively.[56−59] However, it could be more difficult to conclude on the quality of the contact from those modes because those Raman peaks are weak and close to the excitation line.[56,59]

Our method is expected to be very useful for studying vdW-induced epitaxial growth of two-dimensional materials. This approach can be used to examine the mechanical interaction on a nanoscale level, which dominates the layer growth on top of two-dimensional layers lying below. For instance, for the MoS_2 grown on mica,[51] the reported $E_{2g}{}^1$ and A_{1g} modes both show a blue shift compared to normal bare ones. According to our protocol, compared to bare MoS_2 (~384 cm^{-1}), the reported $E_{2g}{}^1$ has a blue shift of about 3 cm^{-1}, indicating an in-plane compression of ~1.42%. The compression level is very close to the estimation (1.5%) reported in ref 37. Meanwhile, the blue shift of A_{1g} observed in ref 37 indicates a firm contact between mica and MoS_2, which provides direct evidence of a vdW-driven force during growth.

CONCLUSION

In this work, we present a Raman-based strategy to probe the interfacial contact in a two-dimensional crystal heterostructure containing a TMDC crystal. Here, MoS_2 was used as a reference, while graphene, WS_2, and mica acted as the other component at the interface. We found that the Raman modes of the TMDC crystal are very sensitive to the interfacial strain and quality of the contact. According to our protocol, in a graphene/MoS_2 heterostructure, a high-quality interfacial contact is obtained when graphene is compressed by 0.1%, and MoS_2 is stretched by 0.3%. A similar result is observed when graphene is encapsulated between the Si/SiO_2 substrate and MoS_2. In contrast, we show by Raman spectroscopy that it is more difficult to obtain a smooth and clean interface when MoS_2 is placed on mica. The interfacial contact can be strongly improved by tapping the surface with the AFM tip, as confirmed by Raman spectroscopy.

In conclusion, we describe a noncontact and rapid approach based on the Raman modes of MoS_2 to investigate the quality of the contact in a heterostructure. As 2-D material heterostructure technology moves to the next level and devices are produced on a large scale, either by direct growth or by transfer methods, we believe this method to be a very useful, high-throughput approach to optimizing the fabrication processes of those devices and generally in improving the design of new heterostructures, for example, selecting the best combination of crystals, growth conditions, substrate choice, *etc*.

EXPERIMENTAL SECTION

Heterostructures consisting of MoS_2 on top of or below a selection of crystals including graphene and mica were produced by the well-known "dry" transfer technique.[5,60] The structures were produced as follows: first a target crystal is deposited onto a freshly cleaned Si/SiO_2 (290 nm) substrate *via* micromechanical exfoliation. The flakes produced are of high quality; that is, they are defect-free. The material that has to be transferred is deposited onto a double-layer polymer stack, and the bottom polymer layer is dissolved, leaving a free floating membrane which can be inverted and aligned with micrometer accuracy. The flakes are then brought into contact, and the final polymer layer is dissolved. In all steps of the transferring, the temperature of the MoS_2 is kept below 60 °C to avoid oxidation effects, which may occur at elevated temperatures.

All Raman spectra were collected by an inVia Renishaw spectrometer with an excitation wavelength of 514.5 nm (2.41 eV) under a 100× objective. To avoid any thermal damage, the collection time was 1 s, which is the same as was used for collecting the Raman maps. A grating of 2400 line/mm was used and provided a resolution of 1 cm^{-1}. The laser power was well below 1 mW to avoid thermal damage in air.

Conflict of Interest: The authors declare no competing financial interest.

Acknowledgment. K.-G.Z. acknowledges the Royal Society in the framework of the Newton international fellowship. This project is partially supported by the U.S. Army Research Office (ARO). The authors thank useful discussions with C. Rice and K.S. Novoselov. F.W acknowledges support from the Royal Academy of Engineering.

Supporting Information Available: Additional data including experimental details on AFM treatment, the calculation of strains, and Raman maps of several heterostructures are presented in the Supporting Information. This material is available free of charge *via* the Internet at http://pubs.acs.org.

REFERENCES AND NOTES

1. Bhattacharya, P. *Semiconductor Optoelectronic Devices*; Prentice Hall: New York, 1994.
2. Wallis, R. F. *Semiconductor Physics and Applications*; Oxford University Press: Oxford, 2000.
3. Novoselov, K. S.; Jiang, D.; Schedin, F.; Booth, T. J.; Khotkevich, V. V.; Morozov, S. V.; Geim, A. K. Two-Dimensional Atomic Crystals. *Proc. Natl. Acad. Sci. U.S.A.* **2005**, *102*, 10451–10453.
4. Geim, A. K.; Grigorieva, I. V. van der Waals Heterostructures. *Nature* **2013**, *499*, 419–425.
5. Ponomarenko, L. A.; Geim, A. K.; Zhukov, A. A.; Jalil, R.; Morozov, S. V.; Novoselov, K. S.; Grigorieva, I. V.; Hill, E. H.; Cheianov, V. V.; Fal'ko, V. I.; *et al.* Tunable Metal-Insulator Transition in Double-Layer Graphene Heterostructures. *Nat. Phys.* **2011**, *7*, 958–961.
6. Britnell, L.; Gorbachev, R. V.; Jalil, R.; Belle, B. D.; Schedin, F.; Mishchenko, A.; Georgiou, T.; Katsnelson, M. I.; Eaves, L.; Morozov, S. V.; *et al.* Field-Effect Tunneling Transistor Based on Vertical Graphene Heterostructures. *Science* **2012**, *335*, 947–950.
7. Zan, R.; Ramasse, Q. M.; Jalil, R.; Georgiou, T.; Bangert, U.; Novoselov, K. S. Control of Radiation Damage in MoS_2 by Graphene Encapsulation. *ACS Nano* **2013**, *7*, 10167–10174.
8. Roy, K.; Padmanabhan, M.; Goswami, S.; Sai, T. P.; Ramalingam, G.; Raghavan, S.; Ghosh, A. Graphene–MoS_2 Hybrid Structures for Multifunctional Photoresponsive Memory Devices. *Nat. Nanotechnol.* **2013**, *8*, 826–830.
9. Myoung, N.; Seo, K.; Lee, S. J.; Ihm, G. Large Current Modulation and Spin-Dependent Tunneling of Vertical Graphene/MoS_2 Heterostructures. *ACS Nano* **2013**, *7*, 7021–7027.
10. Zhang, W.; Chuu, C.-P.; Huang, J.-K.; Chen, C.-H.; Tsai, M.-L.; Chang, Y.-H.; Liang, C.-T.; Chen, Y.-Z.; Chueh, Y.-L.; He, J.-H.; *et al.* Ultrahigh-Gain Phototransistors Based on Graphene–MoS_2 Heterostructures. *Sci. Rep.* **2014**, *4*, 3826.
11. Georgiou, T.; Jalil, R.; Belle, B. D.; Britnell, L.; Gorbachev, R. V.; Morozov, S. V.; Kim, Y.-J.; Gholinia, A.; Haigh, S. J.; Makarovsky, O.; *et al.* Vertical Field-Effect Transistor Based on Graphene–WS_2 Heterostructures for Flexible and Transparent Electronics. *Nat. Nanotechnol.* **2013**, *8*, 100–103.
12. Shi, Y.; Zhou, W.; Lu, A.-Y.; Fang, W.; Lee, Y.-H.; Hsu, A. L.; Kim, S. M.; Kim, K. K.; Yang, H. Y.; Li, L.-J.; *et al.* van der Waals Epitaxy of MoS_2 Layers Using Graphene as Growth Templates. *Nano Lett.* **2012**, *12*, 2784–2791.
13. Britnell, L.; Ribeiro, R. M.; Eckmann, A.; Jalil, R.; Belle, B. D.; Mishchenko, A.; Kim, Y.-J.; Gorbachev, R. V.; Georgiou, T.; Morozov, S. V.; *et al.* Strong Light–Matter Interactions in Heterostructures of Atomically Thin Films. *Science* **2013**, *340*, 1311–1314.
14. Kretinin, A. V.; Cao, Y.; Tu, J. S.; Yu, G. L.; Jalil, R.; Novoselov, K. S.; Haigh, S. J.; Gholinia, A.; Mishchenko, A.; Lozada, M.; *et al.* Electronic Properties of Graphene Encapsulated with Different Two-Dimensional Atomic Crystals. *Nano Lett.* **2012**, *12*, 3270–3276.
15. Georgiou, T.; Britnell, L.; Blake, P.; Gorbachev, R. V.; Gholinia, A.; Geim, A. K.; Casiraghi, C.; Novoselov, K. S. Graphene Bubbles with Controllable Curvature. *Appl. Phys. Lett.* **2011**, *99*, 093103.
16. Haigh, S. J.; Gholinia, A.; Jalil, R.; Romani, S.; Britnell, L.; Elias, D. C.; Novoselov, K. S.; Ponomarenko, L. A.; Geim, A. K.; Gorbachev, R. Cross-Sectional Imaging of Individual Layers and Buried Interfaces of Graphene-Based Heterostructures and Superlattices. *Nat. Mater.* **2012**, *11*, 764–767.
17. Ferrari, A. C.; Meyer, J. C.; Scardaci, V.; Casiraghi, C.; Lazzeri, M.; Mauri, F.; Piscanec, S.; Jiang, D.; Novoselov, K. S.; Roth, S.; *et al.* Raman Spectrum of Graphene and Graphene Layers. *Phys. Rev. Lett.* **2006**, *97*, 187401.
18. Ferrari, A. C. Raman Spectroscopy of Graphene and Graphite: Disorder, Electron–Phonon Coupling, Doping and Nonadiabatic Effects. *Solid State Commun.* **2007**, *143*, 47–57.
19. Malard, L. M.; Pimenta, M. A.; Dresselhaus, G.; Dresselhaus, M. S. Raman Spectroscopy in Graphene. *Phys. Rep.* **2009**, *473*, 51–87.
20. Dresselhaus, M. S.; Jorio, A.; Hofmann, M.; Dresselhaus, G.; Saito, R. Perspectives on Carbon Nanotubes and Graphene Raman Spectroscopy. *Nano Lett.* **2010**, *10*, 751–758.
21. Raza, H.; Dresselhaus, M. S.; Jorio, A.; Cançado, L. G.; Dresselhaus, G.; Saito, R. Raman Spectroscopy: Characterization of Edges, Defects, and the Fermi Energy of Graphene and sp^2 Carbons. In *Graphene Nanoelectronics*; Springer: Berlin, 2012; pp 15–55.
22. Casiraghi, C.; Hartschuh, A.; Qian, H.; Piscanec, S.; Georgi, C.; Fasoli, A.; Novoselov, K. S.; Basko, D. M.; Ferrari, A. C. Raman Spectroscopy of Graphene Edges. *Nano Lett.* **2009**, *9*, 1433–1441.
23. Casiraghi, C. Raman Spectroscopy of Graphene. In *Spectroscopic Properties of Inorganic and Organometallic Compounds: Techniques, Materials and Applications*; The Royal Society of Chemistry: Oxford, UK, 2012; Vol. 43, pp 29–56.
24. Eckmann, A.; Park, J.; Yang, H.; Elias, D.; Mayorov, A. S.; Yu, G.; Jalil, R.; Novoselov, K. S.; Gorbachev, R. V.; Lazzeri, M.; *et al.* Raman Fingerprint of Aligned Graphene/h-BN Superlattices. *Nano Lett.* **2013**, *13*, 5242–5246.
25. Ferrari, A. C.; Basko, D. M. Raman Spectroscopy as a Versatile Tool for Studying the Properties of Graphene. *Nat. Nanotechnol.* **2013**, *8*, 235–246.
26. Tsu, R. Optical Properties and Raman Scattering in Man-Made Quantum Systems. In *Superlattice to Nanoelectronics*, 2nd ed.; Elsevier: London, 2011; pp 115–142.
27. Late, D. J.; Liu, B.; Matte, H. S. S. R.; Rao, C. N. R.; Dravid, V. P. Rapid Characterization of Ultrathin Layers of Chalcogenides on SiO_2/Si Substrates. *Adv. Funct. Mater.* **2012**, *22*, 1894–1905.
28. Li, H.; Zhang, Q.; Yap, C. C. R.; Tay, B. K.; Edwin, T. H. T.; Olivier, A.; Baillargeat, D. From Bulk to Monolayer MoS_2: Evolution of Raman Scattering. *Adv. Funct. Mater.* **2012**, *22*, 1385–1390.
29. Lee, C.; Yan, H.; Brus, L. E.; Heinz, T. F.; Hone, J.; Ryu, S. Anomalous Lattice Vibrations of Single- and Few-Layer MoS_2. *ACS Nano* **2010**, *4*, 2695–2700.
30. Molina-Sánchez, A.; Wirtz, L. Phonons in Single-Layer and Few-Layer MoS_2 and WS_2. *Phys. Rev. B* **2011**, *84*, 155413.
31. Casiraghi, C.; Hartschuh, A.; Lidorikis, E.; Qian, H.; Harutyunyan, H.; Gokus, T.; Novoselov, K. S.; Ferrari, A. C. Rayleigh Imaging of Graphene and Graphene Layers. *Nano Lett.* **2007**, *7*, 2711–2717.
32. Dawlaty, J. M.; Shivaraman, S.; Chandrashekhar, M.; Rana, F.; Spencer, M. G. Measurement of Ultrafast Carrier Dynamics in Epitaxial Graphene. *Appl. Phys. Lett.* **2008**, *92*, 042116.
33. Klar, P.; Lidorikis, E.; Eckmann, A.; Verzhbitskiy, I. A.; Ferrari, A. C.; Casiraghi, C. Raman Scattering Efficiency of Graphene. *Phys. Rev. B* **2013**, *87*, 205435.
34. Buscema, M.; Steele, G. A.; van der Zant, H. S. J.; Castellanos-Gomez, A. The Effect of the Substrate on the Raman and Photoluminescence Emission of Single Layer MoS_2. *Nano Res.* **2014**, *7*, 1–11.
35. Cai, Y.; Lan, J.; Zhang, G.; Zhang, Y.-W. Lattice Vibrational Modes and Phonon Thermal Conductivity of Monolayer MoS_2. *Phys. Rev. B* **2014**, *89*, 035438.
36. Zabel, J.; Nair, R. R.; Ott, A.; Georgiou, T.; Geim, A. K.; Novoselov, K. S.; Casiraghi, C. Raman Spectroscopy of Graphene and Bilayer under Biaxial Strain: Bubbles and Balloons. *Nano Lett.* **2012**, *12*, 617–621.
37. Li, X. D.; Yu, S.; Wu, S. Q.; Wen, Y. H.; Zhou, S.; Zhu, Z. Z. Structural and Electronic Properties of Superlattice Composed of Graphene and Monolayer MoS_2. *J. Phys. Chem. C* **2013**, *117*, 15347–15353.
38. Ma, Y.; Dai, Y.; Guo, M.; Niu, C.; Huang, B. Graphene Adhesion on MoS_2 Monolayer: An *Ab Initio* Study. *Nanoscale* **2011**, *3*, 3883–3887.
39. Sahoo, S.; Gaur, A. P. S.; Ahmadi, M.; Guinel, M. J. F.; Katiyar, R. S. Temperature-Dependent Raman Studies and Thermal

Conductivity of Few-Layer MoS_2. *J. Phys. Chem. C* **2013**, *117*, 9042–9047.
40. Najmaei, S.; Liu, Z.; Ajayan, P. M.; Lou, J. Thermal Effects on the Characteristic Raman Spectrum of Molybdenum Disulfide (MoS_2) of Varying Thicknesses. *Appl. Phys. Lett.* **2012**, *100*, 013106.
41. Das, A.; Pisana, S.; Chakraborty, B.; Piscanec, S.; Saha, S. K.; Waghmare, U. V.; Novoselov, K. S.; Krishnamurthy, H. R.; Geim, A. K.; Ferrari, A. C.; *et al.* Monitoring Dopants by Raman Scattering in an Electrochemically Top-Gated Graphene Transistor. *Nat. Nanotechnol.* **2008**, *3*, 210–215.
42. Chakraborty, B.; Bera, A.; Muthu, D. V. S.; Bhowmick, S.; Waghmare, U. V.; Sood, A. K. Symmetry-Dependent Phonon Renormalization in Monolayer MoS_2 Transistor. *Phys. Rev. B* **2012**, *85*, 161403.
43. Casiraghi, C.; Pisana, S.; Novoselov, K. S.; Geim, A. K.; Ferrari, A. C. Raman Fingerprint of Charged Impurities in Graphene. *Appl. Phys. Lett.* **2007**, *91*, 233108.
44. Casiraghi, C. Probing Disorder and Charged Impurities in Graphene by Raman Spectroscopy. *Phys. Status Solidi RRL* **2009**, *3*, 175–177.
45. Pisana, S.; Lazzeri, M.; Casiraghi, C.; Novoselov, K. S.; Geim, A. K.; Ferrari, A. C.; Mauri, F. Breakdown of the Adiabatic Born-Oppenheimer Approximation in Graphene. *Nat. Mater.* **2007**, *6*, 198–201.
46. Shi, H.; Yan, R.; Bertolazzi, S.; Brivio, J.; Gao, B.; Kis, A.; Jena, D.; Xing, H. G.; Huang, L. Exciton Dynamics in Suspended Monolayer and Few-Layer MoS_2 2D Crystals. *ACS Nano* **2012**, *7*, 1072–1080.
47. Sachs, B.; Britnell, L.; Wehling, T. O.; Eckmann, A.; Jalil, R.; Belle, B. D.; Lichtenstein, A. I.; Katsnelson, M. I.; Novoselov, K. S. Doping Mechanisms in Graphene–MoS_2 Hybrids. *Appl. Phys. Lett.* **2013**, *103*, 251607.
48. Casiraghi, C. Raman Intensity of Graphene. *Phys. Status Solidi B* **2011**, *248*, 2593–2597.
49. Casiraghi, C. Doping Dependence of the Raman Peaks Intensity of Graphene Close to the Dirac Point. *Phys. Rev. B* **2009**, *80*, 233407.
50. Basko, D. M.; Piscanec, S.; Ferrari, A. C. Electron–Electron Interactions and Doping Dependence of the Two-Phonon Raman Intensity in Graphene. *Phys. Rev. B* **2009**, *80*, 165413.
51. Ji, Q.; Zhang, Y.; Gao, T.; Zhang, Y.; Ma, D.; Liu, M.; Chen, Y.; Qiao, X.; Tan, P.-H.; Kan, M.; *et al.* Epitaxial Monolayer MoS_2 on Mica with Novel Photoluminescence. *Nano Lett.* **2013**, *13*, 3870–3877.
52. Hong, X.; Kim, J.; Shi, S.-F.; Zhang, Y.; Jin, C.; Sun, Y.; Tongay, S.; Wu, J.; Zhang, Y.; Wang, F. Ultrafast Charge Transfer in Atomically Thin MoS_2/WS_2 Heterostructures. *Nat. Nanotechnol.* **2014**, 10.1038/nnano.2014.167.
53. Tongay, S.; Fan, W.; Kang, J.; Park, J.; Koldemir, U.; Suh, J.; Narang, D.; Liu, K.; Ji, J.; Li, J.; *et al.* Tuning Interlayer Coupling in Large-Area Heterostructures with CVD-Grown MoS_2 and WS_2 Monolayers. *Nano Lett.* **2014**, *14*, 3185–3190.
54. Cheng, R.; Li, D.; Zhou, H.; Wang, C.; Yin, A.; Jiang, S.; Liu, Y.; Chen, Y.; Huang, Y.; Duan, X. Electroluminescence and Photocurrent Generation from Atomically Sharp WSe_2/MoS_2 Heterojunction p–n Diodes. *Nano Lett.* **2014**, 10.1021/nl502075n.
55. Lee, C.-H.; Lee, G.-H.; Zande, A. M.; Chen, W.; Li, Y.; Han, M.; Cui, X.; Arefe, G.; Nuckolls, C.; Heinz, T. F.; *et al.* Atomically Thin p–n Junctions with van der Waals Heterointerfaces. *Nat. Nanotechnol.* **2014**, 10.1038/nnano.2014.150.
56. Zhao, Y.; Luo, X.; Li, H.; Zhang, J.; Araujo, P. T.; Gan, C. K.; Wu, J.; Zhang, H.; Quek, S. Y.; Dresselhaus, M. S.; *et al.* Interlayer Breathing and Shear Modes in Few-Trilayer MoS_2 and WSe_2. *Nano Lett.* **2013**, *13*, 1007–1015.
57. Plechinger, G.; Heydrich, S.; Eroms, J.; Weissa, D.; Schuller, C.; Korn, T. Raman Spectroscopy of the Interlayer Shear Mode in Few-Layer MoS_2 Flakes. *Appl. Phys. Lett.* **2012**, *101*, 101906.
58. Zhang, Y.; Zhang, J.; Son, H.; Kong, J.; Liu, Z. Substrate-Induced Raman Frequency Variation for Single-Walled Carbon Nanotubes. *J. Am. Chem. Soc.* **2005**, *127*, 17156–17157.
59. Zhang, X.; Han, W. P.; Wu, J. B.; Milana, S.; Lu, Y.; Li, Q. Q.; Ferrari, A. C.; Tan, P. H. Raman Spectroscopy of Shear and Layer Breathing Modes in Multilayer MoS_2. *Phys. Rev. B* **2013**, *87*, 115413.
60. Dean, C. R.; Young, A. F.; Meric, I.; Lee, C.; Wang, L.; Sorgenfrei, S.; Watanabe, K.; Taniguchi, T.; Kim, P.; Shepard, K. L.; *et al.* Boron Nitride Substrates for High-Quality Graphene Electronics. *Nat. Nanotechnol.* **2010**, *5*, 722–726.